Journal of Physics: Materials

PAPER

Tailoring the triboelectric output of poly-L-lactic acid nanotubes through control of polymer crystallinity

Kalliope Margaronis, Tommaso Busolo, Malavika Nair, Thomas Chalklen and Sohini Kar-Narayan *

Department of Materials Science & Metallurgy, University of Cambridge, Cambridge CB3 0FS, United Kingdom
* Author to whom any correspondence should be addressed.

E-mail: sk568@cam.ac.uk

Keywords: triboelectric materials, energy harvesting, polymer crystallinity, nanotubes, nanogenerator

Supplementary material for this article is available online

OPEN ACCESS

RECEIVED
30 December 2020

REVISED
26 March 2021

ACCEPTED FOR PUBLICATION
14 April 2021

PUBLISHED
7 May 2021

Abstract

Triboelectric devices capable of harvesting ambient mechanical energy have attracted attention in recent years for powering biomedical devices. Typically, triboelectric energy harvesters rely on contact-generated charges between pairs of materials situated at opposite ends of the triboelectric series. However, very few biocompatible polymeric materials exist at the 'tribopositive' end of the triboelectric series. In order to further explore the use of triboelectric energy harvesting devices within the body, it is necessary to develop more biocompatible tribopositive materials and look into ways to improve their triboelectric performance in order to enhance the harvested power output of these devices. Poly-L-lactic acid (PLLA) is a tribopositive biocompatible polymer, frequently used in biomedical applications. Here, we present a way to improve the triboelectric output of nanostructured PLLA through fine control of its crystallinity via a customised template-assisted nanotube (NT) fabrication process. We find that PLLA NTs with higher values of crystallinity (∼41%) give rise to a threefold enhancement of the maximum triboelectric power output as compared to NTs of the same material and geometry but with lower crystallinity (∼13%). Our results thus pave the way for the production of a viable polymeric and biocompatible tribopositive material with improved power generation, for possible use in implantable triboelectric nanogenerators.

1. Introduction

Implantable and wearable medical devices have been a staple of modern medicine since the first pacemaker implantation surgery in 1958 [1]. Since then, many new implants have been developed to help manage a wide range of medical problems, yet replacement of the power sources relies on frequent manual intervention or additional invasive procedures [2, 3]. Triboelectric nanogenerators (TENGs) offer an efficient method to harvest mechanical energy [4], one of the most abundant energy sources within the body, to power the next generation of biomedical devices.

Triboelectric devices operate on the principle of contact electrification [5], whereby two surfaces are brought into contact with one another and electric charge is exchanged between them based on a combination of contact electrification and electrostatic induction. When connected via an external circuit and separated after initial contact, the potential difference between the two surfaces drives the flow of electrons around the circuit. The surfaces can be repeatedly contacted and separated to generate an alternating current in the external circuit that can be used as a source of power. The choice of materials is an important factor in the output of these devices, and is often guided by the triboelectric series [6]. This series lists materials according to their ability to donate electrons (tribopositive materials) or accept electrons (tribonegative materials), when used in a triboelectric device. It was first presented as an empirical series however, more rigorous methods have recently been proposed relating the work function of the contacting materials to the polarity and magnitude of charging [7, 8]. Using materials from opposite ends of the series in a triboelectric energy harvesting device results in a larger exchange of charge upon contact, thereby giving

rise to a larger output power. Currently, the materials choice for triboelectric devices for use in biomedical applications is limited by the lack of suitable biocompatible polymeric tribopositive materials [9]. In comparison, there are several known biocompatible polymeric tribonegative materials such as polydimethylsiloxane and polytetrafluoroethylene (PTFE) [10], and therefore the lack of tribopositive options hinders the progress of implantable triboelectric devices.

Improving the output of triboelectric devices can be achieved through choice of material, surface modification (such as adding micro/nano features or altering the surface chemistry), charge injection, or hybridisation with other energy harvesting technologies [11–14], such as the use of triboelectric and piezoelectric devices in tandem to boost output from mechanical modes that cannot easily be harvested by simple triboelectric devices [15]. However, there are problems with relying solely on surface morphology changes to improve device output. For example, with prolonged use, micro and nanostructured features will eventually wear down and the triboelectric performance enhancement from increased surface area will be lost. Therefore, it is important to also focus on improving the output of the triboelectric materials being used themselves. For materials that can operate safely in a biomedical implant, it is convenient to utilise materials that are already common place in these devices, and to then tailor their properties to improve their position in the triboelectric series. To elevate the position of a material, the magnitude of its surface charge density must be increased [8], improving the transfer of charge between triboelectric layers upon contact. Several methods have been used to do improve the surface potential of polymers such as: forming secondary cross-linked networks within existing polymers [16], aligning polymer chains along fibre axes [17], adding different types of electrolytes to polyvinyl alcohol to form solid polymer electrolytes with different surface potentials [18], changing the applied polarity to the nozzle during electrospinning of polymethyl-methacrylate (PMMA) [19], and controlling the crystallinity of nylon-11 [20].

Poly-L-lactic acid (PLLA) is an attractive option as a tribopositive polymer since it is already commonly used in biomedical applications, including for *in vivo* structures such as ligament and tendon repair, and vascular stents [21, 22]. Polylactic acid (PLA) has previously been reported to be tribopositive and has been used in energy harvesting devices [23–26]. However, in this study, we choose to instead use PLLA which, being piezoelectric [27], possesses a remanent polarisation and therefore a larger surface charge density. PLA, in contrast, is non-piezoelectric and therefore does not possess any remanent polarisation. When PLLA is nanostructured into nanotubes (NTs) of large aspect ratio, due to its piezoelectricity [28–30], a remnant surface charge results from dipolar alignment caused by preferential crystallite orientation along the long axis of the NTs. Importantly, this allows the magnitude of the remanent surface charge to be controlled via polymer crystallinity, as it has been shown that crystalline NTs have higher surface charge than amorphous NTs [30]. This effect of increased surface charge with increased crystallinity has also been observed in polymers such as the α and δ' phases of nylon-11 [20, 31]. However, nanostructured nylon-11 requires the assistance of a rigid anodised aluminium oxide (AAO) template to retain nanowire alignment. On the other hand, nanostructured PLLA does not require such additional mechanical support, which further lends credence to its consideration as a strong candidate for triboelectric applications in biomedical settings [32, 33].

PLLA has previously been used as the tribopositive surface in triboelectric energy harvesters [34–36]. However, these studies mainly focused on methods of altering the surface structure in order to improve surface area, and therefore triboelectric output. The methods used involved etching away areas of the surface using 10 M NaOH to create irregular nanorods, hot-embossing with a template to create micro-scale patterns, and roughening PLLA films with sandpaper. However, none of these studies utilised the ability to control the crystallinity to achieve higher triboelectric output, through the intrinsic and persistent modification of surface potential and mechanical compliance. Therefore, to benefit from the biocompatibility of nanostructured PLLA in implantable TENGs, control of crystallinity is an important route to achieving stable and higher outputs from these generators. In this work, we demonstrate how the tailoring of crystallinity can improve the triboelectric performance of PLLA NTs in mechanical energy harvesting applications. Our work suggests that PLLA can provide a viable polymeric and biocompatible tribopositive material for possible use in implantable TENGs.

2. Materials and methods

2.1. Fabrication of PLLA nanotubes *via* melt-press template wetting

Three PLLA (mol wt 85 000–160 000) pellets from Sigma Aldrich were used to fabricate each NT array. Following the process outlined in figure 1(a), these pellets were melted using a hot stage at 215 °C and then manually pressed into a nanoporous template—13 mm AAO template (200 nm pore diameter, WHA68097023). The prepared samples were then annealed at 120 °C on the hot stage for 1.5, 5 or 10 min depending on the desired crystallinity. The annealed samples were then immediately quenched in ice water.

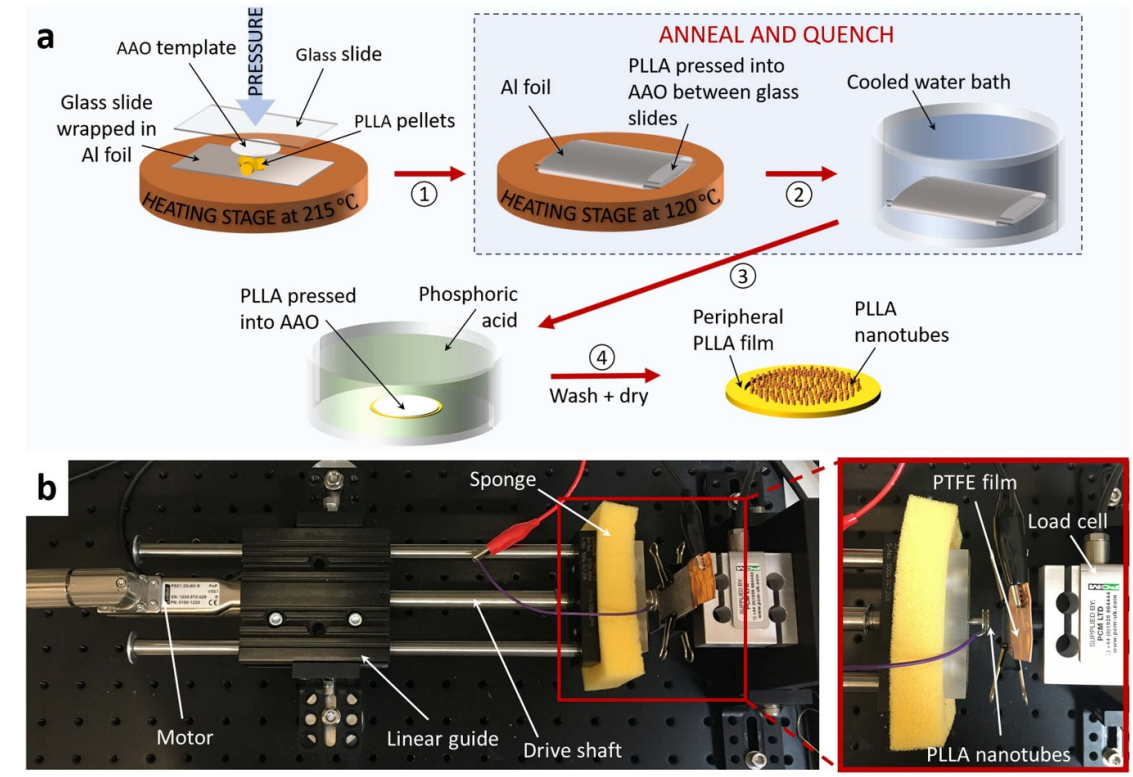

Figure 1. (a) Fabrication of PLLA NTs using melt press template wetting. (b) Linear motor setup for testing triboelectric devices. The sponge is used to prevent decreased contact area between the surfaces due to imperfections in the mounting angle of the samples. This is achieved by increasing the compliance of the system.

To free the NTs from the AAO template, the samples were etched for 4 h in 40% v/v phosphoric acid before being washed in DI water and left to dry. The resulting samples were comprised of vertically aligned arrays of PLLA NTs.

2.2. Evaluation of polymer crystallinity using x-ray diffractometry (XRD)

XRD scans were carried out on the PLLA NTs using a Bruker D8 diffractometer in Bragg−Brentano geometry with a Cu−Kα source ($\lambda = 1.5406$ Å). Scans were taken between $2\theta = 8°$–$35°$ to ensure key crystalline peaks were captured. The scans were analysed in Origin 2020 software. The 'Fit Peaks Pro' function was used to fit the peaks in order to calculate the crystallinity of each sample. Crystallinity was calculated by comparing the relative areas under the curve of crystalline and amorphous peaks, following the relationship:

$$X_{\mathrm{C}} = \frac{I_{\mathrm{c}}}{I_{\mathrm{c}} + I_{\mathrm{a}}}$$

where X_{c} is the crystalline fraction and I_{c} and I_{a} are the total area of amorphous and crystalline peaks, respectively.

2.3. Triboelectric power output measurement

The electrical output of the PLLA NTs in a TENG configuration was tested using a 100 μm thick PTFE film (Goodfellow 630-643-79) as the counter tribonegative material. PTFE is a tribonegative polymer that has been previously used in implanted nanogenerators [37, 38] and is commonly used as a coating for medical implants and as tubing within implanted devices [39]. The PLLA NTs occupied a disc shaped sample of area 176 mm^2. The rear film of the PLLA NTs was coated with Au using a Emitech 550 sputter coater to create a conducting electrode of resistance of ~4 Ω. The NTs were then mounted to a conductive sample holder using double sided copper tape. Double sided copper tape was also stuck to the back of the PTFE film to act as an electrode and to hold it to a stiff substrate, a schematic of which is given in figure 3(d). The sample comprising an array of vertically aligned PLLA NTs was periodically brought into contact with the PTFE film using an oscillating linear motor (figure 1(b)). The applied force was ~2 N and the frequency of oscillation of 1.6 Hz, while the maximum separation between the materials was 10 mm.

Samples were allowed to oscillate for 40 min (periodically making contact and separating) before measurements were taken, in order to stabilise the triboelectric output by allowing the surfaces to reach

maximum charge density. Output voltage was recorded with a multimeter (Keithley 2002) and output current was recorded with a picoammeter (Keithley 6487). Two devices of each crystallinity were tested and their root mean square (RMS) current was found using the 'Find Peaks' function from the Python 3.7 SciPy library and the following equation:

$$f_{\mathrm{RMS}} = \sqrt{\frac{1}{T_2 - T_1}\int_{T_1}^{T_2} [f(t)]^2 \mathrm{d}t}$$

where $f(t)$ is the recorded voltage or current data, $T_2 - T_1$ is the period and dt is the median sampling time of the recording equipment. RMS current was then used to calculate the power output (P_{av}) across a range of applied resistive loads (R) using $P_{\mathrm{av}} = {I_{\mathrm{RMS}}}^2 \times R$.

2.4. Scanning electron microscopy

All images were taken using a Hitachi TM303PLUS desktop microscope using backscattered electrons at 15 kV.

3. Results and discussion

PLLA NTs were fabricated using the melt-press template wetting method previously described by Smith *et al* [33]. However, instead of annealing the NTs for an hour in a furnace, they were instead placed on a 120 °C hot plate for up to 10 min and then immediately quenched in ice water. Altering the annealing time by a few minutes resulted in fine control of crystallinity, while keeping the length of the NTs the same (22 ± 1 μm). The annealing treatment was used to induce crystallisation within the NTs, and the annealing time served to control the degree of crystallisation. A schematic of this process is given in figure 1(a), which illustrates that the manufactured samples are an array of PLLA NTs held together by a residual PLLA film on the underside of the NTs, from where the melt infiltrated the templates. Figure 1(b) shows the linear motor setup used to measure the triboelectric output of the PLLA NT samples with different polymer crystallinities, in order to study the effect of crystallinity on triboelectric performance of the PLLA NTs. A scanning electron microscope (SEM) image of a typical NT array as viewed from the top following removal of the template is shown in supplementary figure S1 (available online at stacks.iop.org/JPMATER/4/034010/mmedia).

As seen in figure 2, when annealed at the constant temperature of 120 °C, the crystallinities as obtained from XRD are seen to increase monotonically with annealing time, reaching a maximum at approximately 40% crystallinity. This is higher than the crystallinity achievable in films at the same annealing temperature, even at longer annealing times (supplementary figure S2(a)). In this work, we therefore demonstrate the ability to tune the lower range of crystallinities with annealing time. The exact values of the crystallinities reported in literature can vary depending on the method of crystallinity measurement (for instance XRD as compared with differential scanning calorimetry), and the deconvolution of the amorphous halo from the crystalline peaks [40]. In spite of these differences, the trends obtained appear consistent with the crystallinities obtained by Smith *et al* [33], with the results from this work suggesting that high crystallinity in PLLA NTs can be achieved at much lower annealing times than previously demonstrated. Furthermore, the maximum crystallinity observed with this process is consistent with the maximum achievable crystallinities reported in the literature for PLLA [40–42].

Since the PLLA NTs remain vertical during measurement, a family of peaks is seen in XRD scans. This is due to the preferential alignment of NTs that leads to an overall preferred crystal orientation of the sample. Only the lattice planes with scattering vectors lying normal to the surface of the sample produce peaks in the XRD geometry used. Therefore, theoretically, a perfectly oriented sample of NTs is expected to contain missing peaks in its XRD traces. However, any deviation from vertical NT alignment during sample characterisation, or imperfect crystallite orientation within the NTs can result in these peaks appearing in the XRD spectra, albeit at lower intensity. Prior investigations on the texture of melt-wetted PLLA NTs have revealed an alignment of PLLA crystallites parallel to the <001> crystal direction (i.e. along the fibre axis), with little evidence to support radial alignment of the polymer chains through the melt-press template wetting adopted here [33].

Three different annealing times were used to fabricate vertically aligned PLLA NT arrays of different crystallinity to study the effect on triboelectric output: 10, 5 and 1.5 min, corresponding to $41 \pm 1\%$, $28 \pm 1\%$ and $13 \pm 2\%$ crystallinity respectively. To prepare the samples for testing in a triboelectric device the peripheral PLLA film around the base of the NTs was removed, leaving only the film directly underneath and attached to the NTs to be coated with a gold electrode. Using a linear motor, the NTs were then periodically oscillated against a tribonegative PTFE film with Cu tape as the counter electrode, as shown in

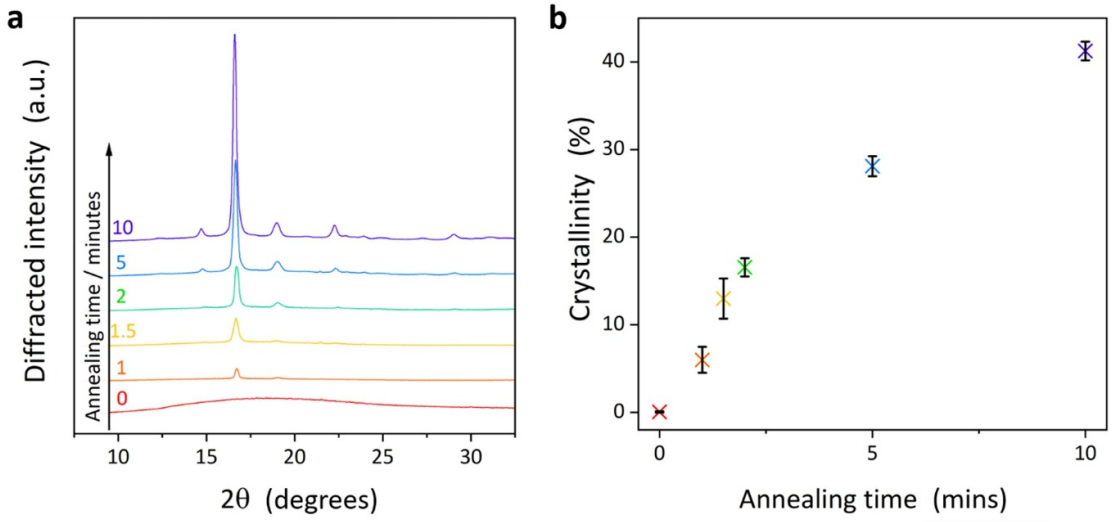

Figure 2. Crystallinity of PLLA NTs when annealed for different lengths of time. (a) XRD traces of a typical sample at each annealing time. (b) Calculated crystallinity using XRD spectra.

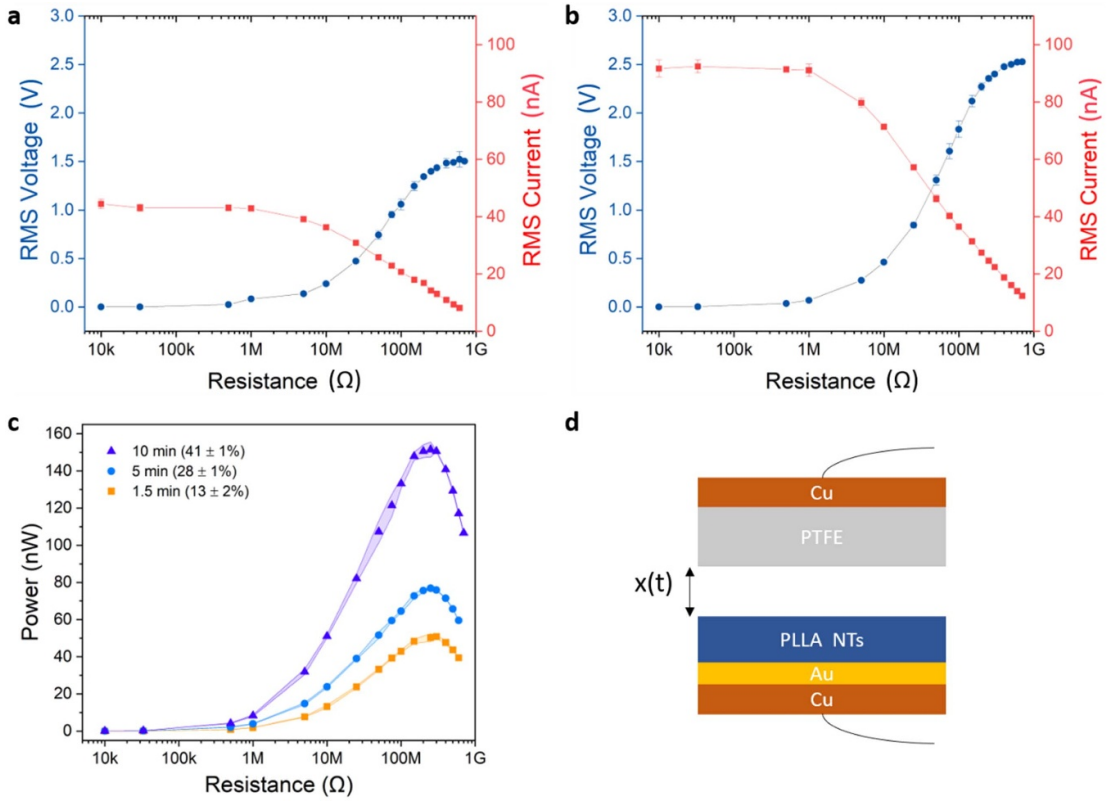

Figure 3. Triboelectric performance of PLLA NTs in an energy harvesting device with PTFE film as the tribonegative counter material. (a) RMS voltage and current of PLLA NTs annealed for 1.5 min (13 ± 2% crystalline) across several load resistances. (b) RMS voltage and current of PLLA NTs annealed for 10 min (41 ± 1% crystalline) across several load resistances. (c) RMS power output of triboelectric devices using PLLA NTs annealed for different times with crystallinities given in the legend. (d) Schematic of triboelectric devices tested.

figure 3(d). These two electrodes are necessary for electrostatic induction during contact and separation of the two dielectric triboelectric surfaces.

Open-circuit voltage (V_{OC}) and short-circuit current (I_{SC}) were measured for each crystallinity as they are commonly used as a benchmark for the performance of TENGs, the values of which are given in table 1. Recently, a non-grounded method of measuring V_{OC} has been proposed by Zhang *et al* [43] which gives a more accurate value of the output as there is no charge leakage to ground. However, the grounded method

Table 1. V_{OC} and I_{SC} results of the three tested values of crystallinity of PLLA NTs.

Annealing time (min)	Crystallinity (%)	V_{OC} (V)	I_{SC} (nA)
1.5	13 ± 2	5.04 ± 0.06	380 ± 30
5	28 ± 1	6.0 ± 0.2	680 ± 60
10	41 ± 1	8.57 ± 0.08	960 ± 30

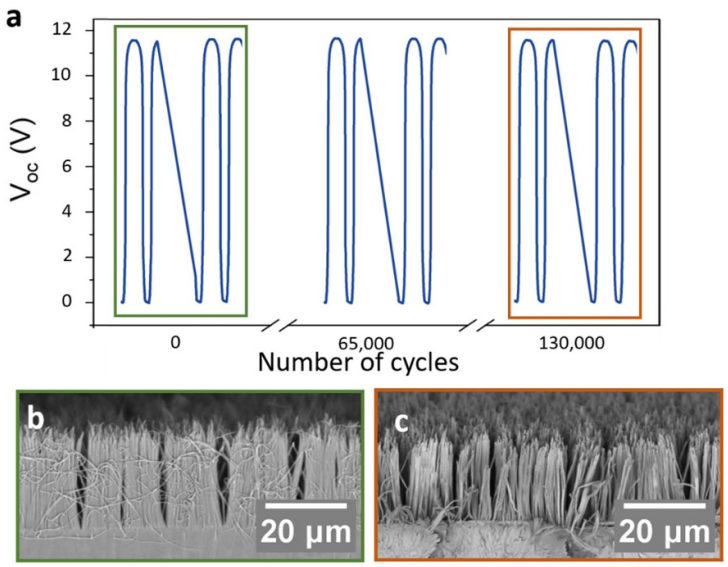

Figure 4. (a) Open circuit voltage of 41 ± 1% crystalline PLLA NTs across several cycles. The same behaviour was seen in samples of lower crystallinity. (b) Cross section of NTs before use in and (c) after use in a TENG for 130 000 cycles.

has been used here for simplicity as we are concerned with the trend in V_{OC} as a function of polymer crystallinity, rather than the exact value of V_{OC}. Both V_{OC} and I_{SC} were found to increase with crystallinity. In order to test the application of PLLA based TENGs for medical devices, the voltage versus time curves of three capacitors (1 μF, 10 μF, 100 μF) were recorded as they were charged by the rectified current of the TENG when driven at 1.6 Hz (supplementary figure S3(a)). The TENG was also tested as a finger bend sensor to demonstrate sensing applications (supplementary figure S3(b)).

To further characterise the effect of crystallinity, the RMS voltage (V_{RMS}) and current (I_{RMS}) of the different crystallinities were measured across a range of applied load resistances. During these measurements the relative humidity was recorded to ensure it remained within a ± 1.5% band across all triboelectric experiments in order to help minimise the effect of environmental factors [44]. RMS is used instead of peak-to-peak or peak electrical output values as it represents the useful current and voltage value that would be supplied by an equivalent DC device. Figures 3(a) and (b) show the V_{RMS} and I_{RMS} of samples annealed for 1.5 and 10 min, respectively. The PLLA NTs with higher crystallinity show an increase in output voltage and current across the range of applied resistances compared to NTs of the same material with lower crystallinity. As shown in figure 3(c), there was a clear increase in the average triboelectric power output as the crystallinity of the PLLA NTs was increased. This can be observed with the threefold increase in power output at the maximum power point (MPP) from 50.9 ± 0.8 nW at 13% crystallinity to 151 ± 4 nW at 41% crystallinity. The MPP also decreased from 300 MΩ to 250 MΩ with increasing crystallinity. This decrease in resistance is beneficial in practice, since devices that could be powered by TENGs are typically of low impedance, resulting in better impedance matching [39].

Figures 4(b) and (c) show representative SEM images of the NTs with the highest crystallinity (∼41%) before and after continuous use in a TENG, along with the voltage output over 130 000 cycles. There was little observed change to the morphology of the surface of the PLLA NTs, and this was the case for all crystallinities studied. This confirms that the nanostructure created was stable, as was the corresponding electrical output, with only a decrease in performance of 0.38%, highlighting the stable fatigue performance of the PLLA NT arrays in TENG applications. This was not the case for PLLA films, where after 130 000 cycles output had decreased from the initial value by 8.8% (supplementary figure S4).

The increase in triboelectric output with increase in crystallinity of PLLA NTs may be attributed to a few concurrent changes in their electromechanical properties such as their elastic compliance and surface potential, as has been previously observed [30]. The annealing process may also influence the texture of the

crystallites within the NTs, allowing for the preferential growth of crystallites oriented along the chain axes. In an investigation of the elastic compliance and surface potential of amorphous and crystalline PLLA NTs by Smith *et al*, crystallisation was accompanied with a threefold reduction in elastic compliance, and a smaller but significant increase in the surface potential [30]. A lower elastic compliance allows for greater retention of the nanostructured surface of the NT array during contact in a TENG, allowing for increased charge exchange. At the same time, as previously discussed, a greater surface potential would result in a larger exchange of charge during tapping between the NTs and the counter material. In turn, this results in a greater induced potential difference between the two electrodes of the TENG. Measurements of surface potential (supplementary figure S5) and further tests involving the replacement of the PTFE counter materials with copper (supplementary figure S6) confirmed the tribopositive nature of PLLA NTs and the increase in tribopositivity with increased crystallinity, although the difference in measured potential between them is small (less than 0.2 V). This suggests that the observed effect of crystallinity on triboelectric output is possibly driven by a combination of the increasing surface potential effect with increasing crystallinity, and the lower compliance of the higher crystallinity NTs.

4. Conclusions

In this work, we investigate for the first time the effect of polymer crystallinity on the triboelectric output of PLLA NTs grown by a template-assisted melt-pressing method. We have shown that the crystallinity of PLLA NTs can be finely controlled by altering the annealing time at a constant temperature of 120 °C, following the infiltration of the melt into the pores of a nanoporous template. XRD analysis of the PLLA NTs showed that the NTs had crystallinity of 41 ± 1%, 28 ± 1% and 13 ± 2%, when annealed for 10, 5 and 1.5 min, respectively. These changes in crystallinity were found to have occurred over relatively short periods of time as compared to previous methods which required an hour to achieve similar levels of crystallinity. Importantly, we have demonstrated that, while maintaining device geometry, the degree of crystallinity influences the triboelectric power output, with the most crystalline samples exhibiting the highest power at the MPP. On the basis of these results, we conclude that highly crystalline PLLA NTs are ideal candidates as stable tribopositive materials in TENGs, and are particularly well-suited for implantable biomedical applications due to the inherent biocompatible nature of PLLA.

Data availability statement

Supporting data for this paper is available at the DSpace@Cambridge data repository (https://doi.org/10.17863/CAM.68607).

Acknowledgments

S K-N acknowledges support from the Centre of Advanced Materials for Integrated Energy Systems 'CAM-IES' Grant No. EP/P007767/1. K M and T C acknowledges funding from an EPSRC Doctoral Training Partnership studentship (Grant No. EP/R513180/1). T B acknowledges funding from the EPSRC Cambridge NanoDTC, Grant No. EP/G037221/1. M N acknowledges Emmanuel College (University of Cambridge) for funding.

ORCID iDs

Tommaso Busolo https://orcid.org/0000-0003-1815-9557
Malavika Nair https://orcid.org/0000-0002-5229-8991
Sohini Kar-Narayan https://orcid.org/0000-0002-8151-1616

References

[1] van Hemel N M and van der Wall E E 2008 8 October 1958, D day for the implantable pacemaker *Netherlands Heart J.* **16** S3–S4
[2] Poole J E *et al* 2010 Complication rates associated with pacemaker or implantable cardioverter-defibrillator generator replacements and upgrade procedures *Circulation* **122** 1553–61
[3] Gould P A and Krahn A D (Canadian Heart Rhythm Society Working Group on Device Advisories) 2006 Complications associated with implantable cardioverter-defibrillator replacement in response to device advisories *JAMA* **295** 1907–11
[4] Chen J and Wang Z L 2017 Reviving vibration energy harvesting and self-powered sensing by a triboelectric nanogenerator *Joule* **1** 480–521
[5] Fan F-R, Tian Z-Q and Lin Wang Z 2012 Flexible triboelectric generator *Nano Energy* **1** 328–34
[6] Wang Z L 2014 Triboelectric nanogenerators as new energy technology and self-powered sensors—principles, problems and perspectives *Faraday Discuss.* **176** 447–58

[7] Zou H *et al* 2020 Quantifying and understanding the triboelectric series of inorganic non-metallic materials *Nat. Commun.* **11** 1
[8] Zou H *et al* 2019 Quantifying the triboelectric series *Nat. Commun.* **10** 1
[9] Wang R, Gao S, Yang Z, Li Y, Chen W, Wu B and Wu W 2018 Engineered and laser-processed chitosan biopolymers for sustainable and biodegradable triboelectric power generation *Adv. Mater.* **30** 1706267
[10] Mi H-Y, Li H, Jing X, He P, Feng P-Y, Tao X, Liu Y, Liu C and Shen C 2020 Silk and silk composite aerogel-based biocompatible triboelectric nanogenerators for efficient energy harvesting *Ind. Eng. Chem. Res.* **59** 12399–408
[11] Kim D W, Lee J H, Kim J K and Jeong U 2020 Material aspects of triboelectric energy generation and sensors *npg Asia Mater.* **12** 1
[12] Zhang R and Olin H 2020 Material choices for triboelectric nanogenerators: a critical review *EcoMat* **2** e12062
[13] Jing Q and Kar-Narayan S 2018 Nanostructured polymer-based piezoelectric and triboelectric materials and devices for energy harvesting applications *J. Phys. Appl. Phys.* **51** 303001
[14] Choi Y S, Kim S W and Kar-Narayan S 2021 Materials-related strategies for highly efficient triboelectric energy generators *Adv. Energy Mater.* **11** 2003802
[15] Zhao C, Zhang Q, Zhang W, Du X, Zhang Y, Gong S, Ren K, Sun Q and Wang Z L 2019 Hybrid piezo/triboelectric nanogenerator for highly efficient and stable rotation energy harvesting *Nano Energy* **57** 440–9
[16] Liu Y, Wang X, Yan Y, Rao Z, Chen H and Guo T 2020 A novel post-processed surface modified double-network polymer layer for a triboelectric nanogenerator *J. Mater. Chem.* A **8** 6328–36
[17] Ho D H *et al* 2020 $\beta-$phase-preferential blow-spun fabrics for wearable triboelectric nanogenerators and textile interactive interface *Nano Energy* **77** 105262
[18] Shi L *et al* 2019 Enhanced performance triboelectric nanogenerators based on solid polymer electrolytes with different concentrations of cations *Nano Energy* **64** 103960
[19] Busolo T, Ura D P, Kim S K, Marzec M M, Bernasik A, Stachewicz U and Kar-Narayan S 2019 Surface potential tailoring of PMMA fibers by electrospinning for enhanced triboelectric performance *Nano Energy* **57** 500–6
[20] Choi Y S, Kim S K, Smith M, Williams F, Vickers M E, Elliott J A and Kar-Narayan S 2020 Unprecedented dipole alignment in $\alpha-$phase nylon-11 nanowires for high-performance energy-harvesting applications *Sci. Adv.* **6** eaay5065
[21] Abizaid A and Costa J R 2010 New drug-eluting stents *Circ. Cardiovasc. Interv.* **3** 384–93
[22] Longo U G, Lamberti A, Maffulli N and Denaro V 2010 Tendon augmentation grafts: a systematic review *Br. Med. Bull.* **94** 165–88
[23] Gong S, Zhang B, Zhang J, Wang Z L and Ren K 2020 Biocompatible poly(lactic acid)-based hybrid piezoelectric and electret nanogenerator for electronic skin applications *Adv. Funct. Mater.* **30** 1908724
[24] Pan R, Xuan W, Chen J, Dong S, Jin H, Wang X, Li H and Luo J 2018 Fully biodegradable triboelectric nanogenerators based on electrospun polylactic acid and nanostructured gelatin films *Nano Energy* **45** 193–202
[25] Chen G, Xu L, Zhang P, Chen B, Wang G, Ji J, Pu X and Wang Z L 2020 Seawater degradable triboelectric nanogenerators for blue energy *Adv. Mater. Technol.* **5** 2000455
[26] Qiao H, Zhang Y, Huang Z, Wang Y, Li D and Zhou H 2018 3D printing individualized triboelectric nanogenerator with macro-pattern *Nano Energy* **50** 126–32
[27] Smith M and Kar-Narayan S 2021 Piezoelectric Polymers: theory, challenges and opportunities *Int. Mater. Rev.* (https://doi.org/10.1080/09506608.2021.1915935)
[28] Smith M, Calahorra Y, Jing Q and Kar-Narayan S 2017 Direct observation of shear piezoelectricity in poly-l-lactic acid nanowires *APL Mater.* **5** 074105
[29] Calahorra Y, Smith M, Datta A, Benisty H and Kar-Narayan S 2017 Mapping piezoelectric response in nanomaterials using a dedicated non-destructive scanning probe technique *Nanoscale* **9** 19290–7
[30] Smith M *et al* 2020 Poly-l-lactic acid nanotubes as soft piezoelectric interfaces for biology: controlling cell attachment via polymer crystallinity *ACS Appl. Bio Mater.* **3** 2140–9
[31] Sik Choi Y, Jing Q, Datta A, Boughey C and Kar-Narayan S 2017 A triboelectric generator based on self-poled nylon-11 nanowires fabricated by gas-flow assisted template wetting *Energy Environ. Sci.* **10** 2180–9
[32] Choi Y S and Kar-Narayan S 2020 Nylon-11 nanowires for triboelectric energy harvesting *EcoMat* **2** e12063
[33] Smith M, Lindackers C, McCarthy K and Kar-Narayan S 2019 Enhanced molecular alignment in poly-l-lactic acid nanotubes induced via melt-press template-wetting *Macromol. Mater. Eng.* **304** 1800607
[34] Wang Q, Chen M, Li W, Li Z, Chen Y and Zhai Y 2017 Size effect on the output of a miniaturized triboelectric nanogenerator based on superimposed electrode layers *Nano Energy* **41** 128–38
[35] Li W, Xu X, Li W, Zhao Y and Chen M 2018 Fabrication, characterization and *in vitro* evaluation of triboelectric nanogenerator based on 317 L stainless steel and polylactic acid *Nanotechnology* **29** 205402
[36] Liu G, Sun J, Chen M, Zhao Y and Li W 2015 The effect of anodized Ti on output performance of biomedical compatible triboelectric nanogenerators used for controlling the degradation of Mg-3 wt% Zn−0.8 wt% Zr *Nanotechnology* **26** 495401
[37] Yu Y, Sun H, Orbay H, Chen F, England C G, Cai W and Wang X 2016 Biocompatibility and *in vivo* operation of implantable mesoporous PVDF-based nanogenerators *Nano Energy* **27** 275–81
[38] Yao G, Kang L, Li J, Long Y, Wei H, Ferreira C A, Jeffery J J, Lin Y, Cai W and Wang X 2018 Effective weight control via an implanted self-powered vagus nerve stimulation device *Nat. Commun.* **9** 1
[39] Zdrahala R J 1996 Small caliber vascular grafts. Part I: state of the art *J. Biomater. Appl.* **10** 309–29
[40] Srithep Y, Nealey P and Turng L-S 2013 Effects of annealing time and temperature on the crystallinity and heat resistance behavior of injection-molded poly(L-lactic acid) *Polym. Eng. Sci.* **53** 580–8
[41] Yin H-Y, Wei X-F, Bao R-Y, Dong Q-X, Liu Z-Y, Yang W, Xie B-H and Yang M-B 2015 High-melting-point crystals of poly(L-lactic acid) (PLLA): the most efficient nucleating agent to enhance the crystallization of PLLA *Cryst. Eng. Comm.* **17** 2310–20
[42] Ribeiro C, Sencadas V, Costa C M, Ribelles J L G and Lanceros-Méndez S 2011 Tailoring the morphology and crystallinity of poly(L-lactide acid) electrospun membranes *Sci. Technol. Adv. Mater.* **12** 015001
[43] Zhang W *et al* 2020 Measuring the actual voltage of a triboelectric nanogenerator using the non-grounded method *Nano Energy* **77** 105108
[44] Dharmasena R D I G, Deane J H B and Silva S R P 2018 Nature of power generation and output optimization criteria for triboelectric nanogenerators *Adv. Energy Mater.* **8** 1802190